View metadata, citation and similar papers at core.ac.uk

brought to you by CORE

provided by Elsevier - Publisher Connector

Cell PRESS

Structure

Article

Structure of a NEMO/IKK-Associating Domain Reveals Architecture of the Interaction Site

Mia Rushe,[1,4] Laura Silvian,[1,4] Sarah Bixler,[1] Ling Ling Chen,[1] Anne Cheung,[1] Scott Bowes,[1,2] Hernan Cuervo,[1] Steven Berkowitz,[1] Timothy Zheng,[1] Kevin Guckian,[1] Maria Pellegrini,[1,3,*] and Alexey Lugovskoy[1,*]

[1]Biogen Idec Inc., Cambridge, MA 02142, USA

[2]Present address: Novartis Institutes for BioMedical Research Inc., Cambridge, MA 02139, USA.

[3]Present address: Dartmouth College, Hanover, NH 03755, USA.

[4]These authors contributed equally to this work.

*Correspondence: maria.m.pellegrini@gmail.com (M.P.), alexey.lugovskoy@biogenidec.com (A.L.)

DOI 10.1016/j.str.2008.02.012

SUMMARY

The phosphorylation of IκB by the IKK complex targets it for degradation and releases NF-κB for translocation into the nucleus to initiate the inflammatory response, cell proliferation, or cell differentiation. The IKK complex is composed of the catalytic IKKα/β kinases and a regulatory protein, NF-κB essential modulator (NEMO; IKKγ). NEMO associates with the unphosphorylated IKK kinase C termini and activates the IKK complex's catalytic activity. However, detailed structural information about the NEMO/IKK interaction is lacking. In this study, we have identified the minimal requirements for NEMO and IKK kinase association using a variety of biophysical techniques and have solved two crystal structures of the minimal NEMO/IKK kinase associating domains. We demonstrate that the NEMO core domain is a dimer that binds two IKK fragments and identify energetic hot spots that can be exploited to inhibit IKK complex formation with a therapeutic agent.

INTRODUCTION

NF-κB is a ubiquitous transcription factor involved in the regulation of cell signaling responses. Its activation can lead to multiple cellular outcomes in a context-dependent manner, including the inflammatory response, cell proliferation, and cell differentiation. Typically, the canonical NF-κB signaling cascade is initiated by such stimuli as tumor necrosis factor α (TNFα), bacterial lipopolysaccharide (LPS), and genotoxic agents. A key regulatory element in this signaling pathway is the multimeric IKK complex, composed of catalytic kinase subunits IKKα and IKKβ, and a regulatory subunit, called NEMO (IKKγ, IKKAP1, and FIP3). The catalytically active IKK complex phosphorylates IκB, leading to IκB degradation and, ultimately, the nuclear translocation of NF-κB. Inhibition of the NF-κB signaling pathway presents therapeutic potential for reducing arthritis, asthma, autoimmune disease, and certain cancers that result from NF-κB hyperactivation (Karin and Delhase, 2000). The TNFα inhibitors Enbrel and Remicade, therapeutics that block stimuli leading to NF-κB activation, have been successful in treating arthritis and other autoimmune diseases. Small molecule inhibitors of IKK complex assembly could offer an alternative mode of inhibition of NF-κB activation and, in addition, provide benefits of oral administration and decreased risk of immunogenicity.

Although IKK complexes that range from 700 to 900 kDa have been isolated (DiDonato et al., 1997; Mercurio et al., 1997; Yamaoka et al., 1998; Zandi et al., 1997), the molecular composition and stoichiometry of the complex is a matter of debate. It is possible that multiple forms of the complex exist, and there is evidence that its composition varies in a stimulus-dependent manner (Solt et al., 2007). Despite this uncertainty, it is well established that NEMO is essential for the activation of the IKK complex in the canonical NF-κB signaling pathway (Bonizzi and Karin, 2004; Makris et al., 2000; Rudolph et al., 2000; Schmidt-Supprian et al., 2000). The IKKα and IKKβ kinases share 52% identity. Each contains a kinase domain, a leucine-zipper motif through which the catalytic subunits dimerize, and a helix-loop-helix domain followed by a C-terminal tail that, when unphosphorylated, interacts with NEMO (Zandi et al., 1997). The predominant form of the complex contains an IKKα/β heterodimer, but both IKKα and IKKβ homodimers (Karin, 1999; Mercurio et al., 1997; Woronicz et al., 1997; Zandi et al., 1998) and, recently, even monomeric IKKα and IKKβ kinases (Fontan et al., 2007) have been reported in association with NEMO. The predicted domain structure of NEMO includes two coiled-coil regions (CC1 and CC2), a leucine zipper (LZ), and a C-terminal zinc finger (ZF) (Figure 1A). The N-terminal CC1 region interacts with the IKK kinase C-terminal tails (Ghosh and Karin, 2002; Leonardi et al., 2000). Although the CC2 and LZ regions of NEMO have been proposed as potential sites of trimerization (Agou et al., 2002) or tetramerization (Tegethoff et al., 2003), the N-terminal domain encompassing CC1 has been reported to exist as a dimer (Marienfeld et al., 2006).

A considerable amount is known about the intermolecular requirements for the association of the IKK C-terminal tail and the N-terminal CC1 region of NEMO. The IKK-binding region of NEMO has recently been confined to residues 47–120 (Marienfeld et al., 2006). Replacement of the phosphoacceptor Ser68 within this region with a phosphoserine mimetic (glutamate) decreased dimerization of NEMO in immunoblot analysis of 293 cell extracts and reduced IKKβ binding in vitro, whereas replacement with cysteine or alanine enhanced the observed dimerization (Palkowitsch et al., 2008). A C-terminal region of IKKβ containing a conserved sequence common to both IKKα and IKKβ

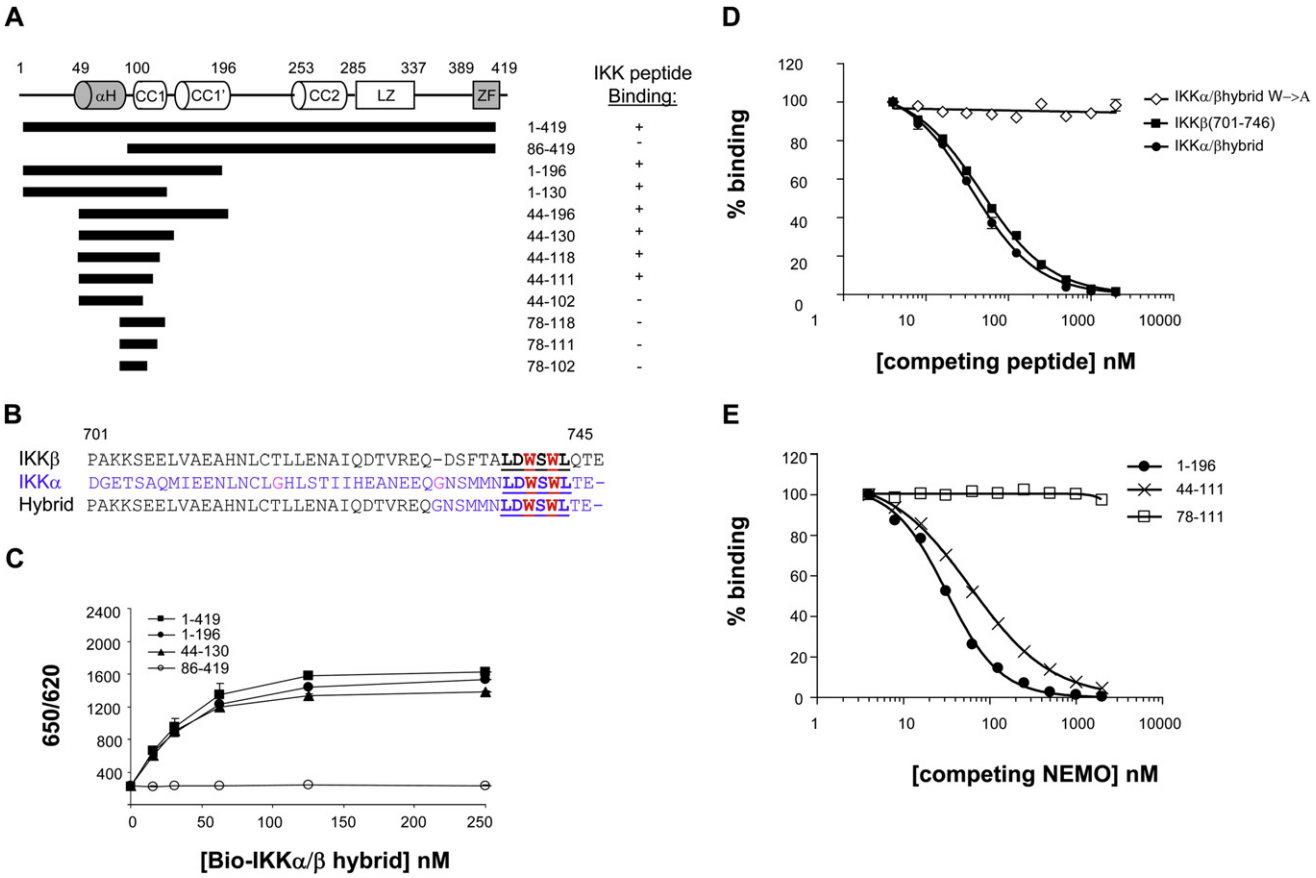

Figure 1. Binding of NEMO and IKK Peptides

(A) Predicted structural regions of NEMO (αH, α helix; CC, coiled-coil; LZ, leucine zipper; ZF, zinc finger) with schematic of recombinant proteins produced; binding to IKK α/β hybrid measured by FRET and denoted by (+) or (−).

(B) Sequence alignment of IKKβ (black), IKKα (blue), and IKKα/β hybrid peptides. Underlined residues indicate those comprising the NEMO-binding domain (NBD). Red indicates the required W residues in the NBD. Magenta indicates helix-breaking residues G717 and G731 of IKKα.

(C) Binding of GST-NEMO proteins to biotinylated-IKK α/β hybrid in FRET assay. Error bars represent the standard deviation from the average.

(D) Untagged peptides titrated into GST-$NEMO_{1–196}$ bound to biotinylated IKKα/β hybrid 44-mer peptide. Error bars represent the standard deviation from the average. Peptide sequences are in Table 1.

(E) Competition binding curves of $NEMO_{44–111}$, $NEMO_{1–196}$, and $NEMO_{78–111}$. Untagged, refolded proteins were titrated into GST-$NEMO_{1–196}$ bound to IKKα/β 44-mer hybrid.

(L_{737}DWSWL$_{742}$), commonly referred to as the NEMO-binding domain (NBD) (May et al., 2000), is critical for complex formation. A cell-permeable peptide containing the NBD sequence prevents formation of the IKK complex (May et al., 2002) and effectively inhibits NF-κB activation in human cancer cell lines (Biswas et al., 2004; Thomas et al., 2002) and in multiple cell-based and animal models of inflammation (May et al., 2000; Tas et al., 2006). Mutational analysis has identified D738, W739, and W741 within the NBD as key binding determinants (May et al., 2002). Furthermore, phosphorylation of S740 within the NBD reduces the association with NEMO (May et al., 2002; Schomer-Miller et al., 2006).

In this study, we have defined the minimal complex of NEMO and IKK using rationally truncated NEMO proteins and IKK-derived fragments. Residues 44–111 of NEMO constitute the minimal IKK interaction domain, and two crystal structures of this domain complexed to IKK kinase fragments are presented. The $NEMO_{44–111}$-IKK peptide complexes observed in the crystal structures as well as a larger N-terminal fragment $NEMO_{1–196}$ are dimeric. The crystal structure reveals the molecular details of the association between NEMO and the IKK kinases, explains how phosphorylation of certain serine residues in this region might affect complex formation, and finally, suggests avenues for the development of targeted small molecule therapeutic agents.

RESULTS

Minimal Binding Domains

A series of truncated IKKα and IKKβ peptides was designed to obtain a NEMO/IKK complex suitable for structural studies. A hybrid IKKα/β peptide was constructed to understand the differences in affinity between IKKα and IKKβ and to serve as a tool for assays. The hybrid peptide (α/β, 44-mer) consists of 30 amino acids derived from the C terminus of the IKKβ sequence (701–730 in IKKβ numbering) followed by 14 amino acids derived from IKKα (731–745 in IKKα numbering), including the conserved NBD hexapepetide LDWSWL (Figure 1B). A biotinylated version

Table 1. IKK Peptide Sequences

IKKα/β hybrid	PAKKSEELVAEAHNLCTLLENAIQDTVR EQGNSMMNLDWSWLTE
IKKβ(701–746)	PAKKSEELVAEAHNLCTLLENAIQDTVREQD QSFTALDWSWLQTE
IKKα/β hybrid (W→A)	PAKKSEELVAEAHNLCTLLENAIQDTVREQ GNSMMNLDASALTE
α/β-28-mer	TLLENAIQDTVREQGNSMMNLDWSWLTE
α/β-19-mer	TVREQGNSMMNLDWSWLTE
α-11-mer	MMNLDWSWLTE
β-11-mer	FTALDWSWLQT

of the hybrid peptide was synthesized to test the affinity of IKK-derived peptides for NEMO proteins using an in vitro fluorescence resonance energy transfer (FRET) assay. In agreement with previously published results (May et al., 2002), full-length $NEMO_{1–419}$ and $NEMO_{1–196}$ both bind to this peptide, whereas $NEMO_{86–419}$ does not (Figure 1C). When tested in a competition format, both the IKKα/β hybrid peptide and an IKKβ-derived peptide (IKKβ [701–746]) bind $NEMO_{1–196}$ with equivalent binding affinities (IC_{50} values of 36 and 47 nM, respectively; Figure 1D). The negative control, an IKKα/β hybrid peptide in which the two tryptophan residues within the NBD hexapeptide sequence were mutated to alanine (IKKα/β hybrid [W→A]; Table 1), did not compete for binding (Figure 1D).

N-terminal truncation of the IKKα/β hybrid peptide resulted in significantly reduced binding to NEMO. The IKKα/β 19-mer and IKKα/β 28-mer peptides bound $NEMO_{1–196}$ with low micromolar affinity, whereas the IKKα 11-mer peptide could not compete with the IKK α/β 44-mer hybrid, up to a concentration of 100 μM (data not shown). Though the IKKα 11-mer peptide did not compete with the IKKα/β 44-mer hybrid, both biotinylated IKKα and IKKβ 11-mer hybrids bound to $NEMO_{1–196}$ in the FRET assay, whereas a D-amino IKKα/β 44-mer hybrid peptide did not (see Figure S1A in the Supplemental Data available with this article online). Furthermore, the biotinylated IKKα 11-mer peptide bound to $NEMO_{1–196}$ can be successfully displaced by the IKKα 11-mer, IKKα/β 19-mer, and IKKα/β 28-mer peptides with IC_{50} values of 39 μM, 20 μM, and 7 μM, respectively (Figure S1B). Given the micromolar affinities of the truncated peptides relative to nanomolar affinities of the longer peptides, the IKKα/β hybrid 44-mer and the IKKβ 45-mer peptides were selected for structural studies.

By use of a rational design approach, $NEMO_{44–111}$ was identified as the minimal region that retains high-affinity binding to IKK-derived peptides. The results of these binding studies are summarized in Figure 1A. NEMO truncation design was guided by previously published results in conjunction with secondary structure prediction results (Combet et al., 2000; Wolf et al., 1997). The NEMO constructs shown in Figure 1A were produced in iterative rounds and were tested for binding to the IKKα/β hybrid peptide. The predicted structured regions within $NEMO_{1–196}$ consist of a helical fragment (49–94) and two coiled-coil regions (103–130 and 136–195) that are collectively referred to as CC1 (Figure 1A). Because it had been shown that $NEMO_{44–419}$ retains IKK-binding activity (May et al., 2000), residue 44 was selected as the N terminus of the first set of truncated NEMO constructs. $NEMO_{1–419}$, $NEMO_{1–196}$, $NEMO_{1–130}$, $NEMO_{44–196}$, and $NEMO_{44–130}$ were produced as N-terminal glutathione S-transferase (GST) fusion proteins and were tested for IKK binding. All bound to biotinylated IKKα/β hybrid peptide in the FRET assay (Figure 1C, $NEMO_{44–196}$ not shown), indicating that neither the N-terminal 44 amino acids nor the C-terminal residues past amino acid 130 are required for IKK binding. C-terminal truncations designed to shorten $NEMO_{44–130}$ sequentially by three helical turns were introduced at residues 118, 111, and 102. $NEMO_{44–118}$ and $NEMO_{44–111}$ retained IKK peptide-binding activity, whereas $NEMO_{44–102}$ did not (Figure S1C). In a third round of design, N-terminal truncations beginning at 78 ($NEMO_{78–118}$, $NEMO_{78–111}$, and $NEMO_{78–102}$) were produced through peptide synthesis but none were capable of competing with $NEMO_{1–196}$ for binding peptide (data not shown) and thus were not considered for subsequent studies. $NEMO_{44–111}$ encompasses the residues required for IKK binding.

Refolding Studies

Although NEMO proteins cleaved from the GST-fusion partner did retain IKK peptide-binding activity (data not shown), these truncated NEMO proteins were of insufficient purity and biochemical homogeneity for use in biophysical studies. Therefore, refolding protocols were developed for $NEMO_{1–196}$ and $NEMO_{44–111}$. Because of poor expression of GST-$NEMO_{44–111}$, the untagged $NEMO_{44–111}$ was expressed in *Escherichia coli* as insoluble inclusion bodies and was refolded in vitro. $NEMO_{1–196}$ was cleaved from the GST-fusion partner, denatured, refolded, and further purified. As a result, the purity of each refolded protein was greater than 90%. Refolded $NEMO_{1–196}$ and $NEMO_{44–111}$ competed similarly with the GST-$NEMO_{1–196}$ in the FRET binding assay with IC_{50} values of 32 nM and 60 nM, respectively (Figure 1E), confirming both that the refolded proteins retain IKK-binding activity and that the properties required for IKK peptide binding are maintained in the much shorter $NEMO_{44–111}$. Although the refolded $NEMO_{44–111}$ was active in the FRET peptide-binding assay, conformational heterogeneity of apo-$NEMO_{44–111}$ was observed by NMR (described in the next section; Figure S2A) and size-exclusion chromatography (SEC) analysis. Refolding of $NEMO_{44–111}$ in the presence of the IKK α/β hybrid peptide resulted in a homogeneous preparation more suitable for analysis using biophysical techniques.

NMR Analyses of NEMO and NEMO/IKK Fragments

NMR was used to further assess the minimal requirements of each fragment to form a homogeneous, well-ordered species for crystallization. NMR spectra were collected and evaluated for features that are consistent with a monodisperse sample with few disordered regions. By use of ^{1}H,^{15}N correlation spectroscopy, ^{15}N-labeled NEMO proteins were screened in the presence or absence of the IKK α/β hybrid peptide, and the NMR spectra were evaluated on the basis of the number of resonances visible, chemical shift dispersion, and line broadening (Page et al., 2005). Proteins starting at residue 1 produced NMR spectra with ~40 very intense crosspeaks with poor dispersion (data not shown), whereas proteins starting at residue 44 did not display this characteristic. This finding was attributed to a disordered N terminus of ~40 residues; therefore, residue 44 was selected as the N-terminal start site for crystallization constructs. Furthermore, spectra of apo-$NEMO_{44–111}$ displayed

 ©2008 Elsevier Ltd All rights reserved

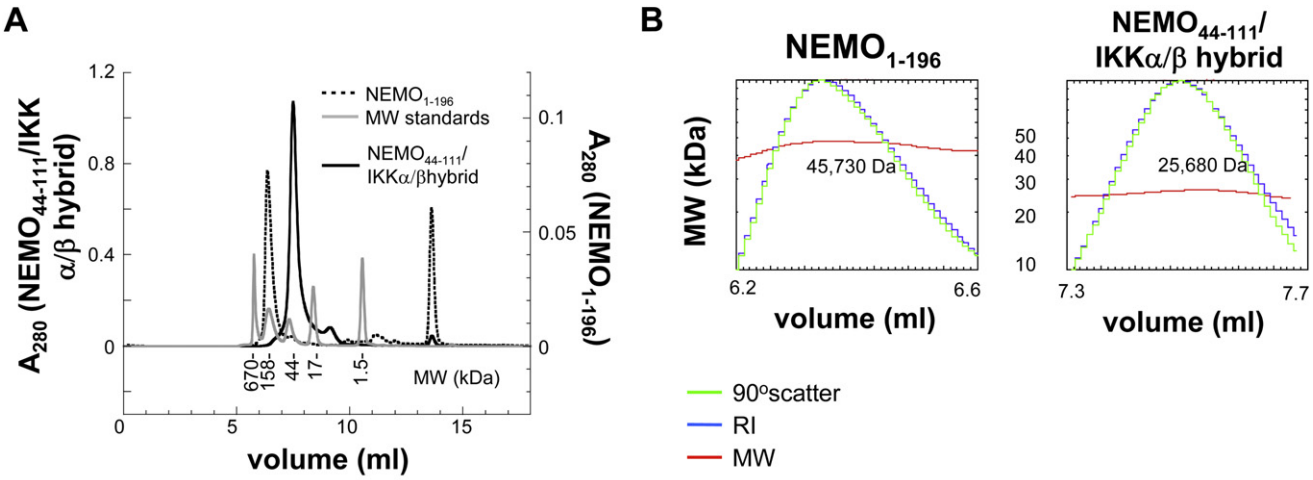

C

	$NEMO_{1-196}$	$NEMO_{44-111}$/ IKKα/βhybrid
Calc. dimer	45,550 Da	27,036 Da
LS/SEC	45,730 Da	25,680 Da
AUC/SE	45,900 Da	25,200 Da

Figure 2. $NEMO_{1-196}$ and $NEMO_{44-111}$/IKKα/β Hybrid Peptide Complex Are Dimeric

(A) Size-exclusion chromatogram of NEMO and molecular weight standards.

(B) Homogeneity plots of regions of the main peak integrated for molecular weight determination by SEC/LS. Normalized traces shown are refractive index (blue) and 90° light scatter (green) and calculated molecular weight (red).

(C) Summary of molecular weight of complexes based on theoretical molecular weight calculation and experimental data.

a small set of severely broadened crosspeaks (Figure S2A), whereas the $^{1}H,^{15}N$ TROSY-HSQC spectrum of $NEMO_{44-111}$ complexed with the IKK α/β hybrid peptide contained the appropriate number of crosspeaks for a single homogeneous species in solution with dispersion characteristic of a folded protein (Figure S2B). $NEMO_{44-111}$/IKK α/β peptide complex, which gave high-quality NMR spectra, also formed crystals.

$NEMO_{1-196}$ and $NEMO_{44-111}$ Are Dimers that Bind IKK with Similar Affinity

$NEMO_{1-196}$ and $NEMO_{44-111}$/IKK α/β hybrid complexes were analyzed using SEC, light scattering, and analytical ultracentrifugation. SEC followed by static light scattering yielded a molecular weight of 45.7 kDa for $NEMO_{1-196}$, which corresponds to a dimer, and 25.7 kDa for the $NEMO_{44-111}$/IKK α/β hybrid peptide complex, which corresponds to two $NEMO_{44-111}$ proteins and two IKK peptides (Figure 2B). Compared with globular protein standards on gel filtration, the apparent molecular weights of the NEMO proteins were much larger than those measured by light scattering (Figure 2A). This finding suggests that the $NEMO_{1-196}$ dimer and the $NEMO_{44-111}$/IKK α/β hybrid complex are elongated. Sedimentation equilibrium analytical ultracentrifugation was also used to measure the molecular weights of the proteins in solution. $NEMO_{1-196}$ and $NEMO_{44-111}$/IKK α/β hybrid peptide complex are single ideal species with molecular weights of 45.9 kDa and 25.2 kDa, respectively (data not shown), a finding that is in agreement with static light scattering results. These data along with the calculated molecular weights of the dimeric $NEMO_{1-196}$ and the tetrameric $NEMO_{44-111}$/IKK α/β hybrid peptide complex are summarized in Figure 2C.

Structure Solution and Architecture of the NEMO/IKK α/β Hybrid and NEMO/IKKβ Complexes

The crystal structures of $NEMO_{44-111}$/IKK α/β hybrid peptide complex (to 2.25 Å resolution) and $NEMO_{44-111}$/IKKβ complex (to 2.2 Å resolution) were determined (Table 2), and representative electron density for the $NEMO_{44-111}$/IKKβ complex is shown in Figure 3. The structures reveal that both protein complexes are heterotetramers consisting of a NEMO dimer and two IKK peptides. In the $NEMO_{44-111}$/IKKα/β hybrid peptide complex, NEMO density extends from residues 49 to 109 in chain B and from residues 49 to 109 in chain D. The IKK peptide density extends from residues 705 to 743 in chain A and from residues 701 to 744 in chain C. The description that follows applies to both the NEMO/IKKβ peptide complex and the NEMO/IKKα/β hybrid peptide complex, unless explicitly stated.

The heterodimeric complex is an elongated and atypical parallel four-helix bundle (Figure 4A). Each NEMO molecule is a crescent-shaped α helix. The helices pack head-to-head to form a dimerization interface at the N and C termini (residues 51–65 and 103–107) with a slit-shaped aperture running down the length of the bundle (Figures 4B, 4D, and 4E). The two IKK peptides bridge across the

Table 2. Data Collection, Phasing, and Refinement Statistics

Data collection									
			IKKα/β hybrid[a]						IKKβ[a]
Space group			$P2_12_12_1$						$P2_12_12_1$
Cell dimensions									
a, *b*, *c* (Å)			41.9, 105.6, 56.7						90, 90, 90
α, β, γ (°)			44.8, 102.8, 50.7						90, 90, 90
			Semet1						Semet2
Phasing	NEMO/IKKβ Native	NEMO/IKKα/β Native	Peak	Inflection	Remote	Peak	Inflection	Remote low E	*Remote High E*
Wavelength (Å)	1.0	1.1	0.9794	0.9796	0.9577	0.9799	0.9799	1.000	0.9577
Resolution (Å)	50–2.20	50–2.25	50–2.5	50–2.5	50–2.5	50–2.4	50–2.4	50–2.4	50–2.4
R_{sym} or R_{merge} (%)[b]	10.3 (56.7)	7.2 (39.6)	6.4 (45.8)	6.7 (48.7)	7.1 (51.7)	6.0 (56.5)	6.1 (59.1)	6.3 (66.6)	6.6 (66.4)
$I/\sigma I$[b]	15.1 (2.2)	28.3 (1.7)	19.5 (2.4)	18.3 (2.1)	16.8 (1.9)	20.8 (2.1)	20.0 (1.8)	18.5 (1.4)	18.5 (1.5)
Completeness (%)[b]	99.1 (95.9)	93.4 (69.4)	99.6 (98.6)	99.4 (96.0)	99.6 (97.5)	98.5 (97.3)	98.5 (96.6)	98.2 (93.3)	98.5 (95.6)
Redundancy	5.3	7.9	3.7	3.8	3.8	3.9	3.9	3.8	3.8
Refinement			$NEMO_{44–111}$/IKKα/β hybrid					$NEMO_{44–111}$/IKKβ hybrid	
Resolution (Å)[b]			38.9–2.25(2.66–2.25)					45.5–2.2 (2.5–2.2)	
No. of reflections[b]			11,119 (587)					11,737(813)	
R_{work}/R_{free} (%)[b]			23.8/28.1 (25.7/35.5)					21.8/29.2 (25.137.3)	
No. of atoms									
Protein			1594					1623	
Water			62					103	
Average *B*-factors (Å^2)			41.3					16.2	
Root mean squared deviations									
Bond lengths (Å)			0.022					0.025	
Bond angles (°)			1.93					2.24	
Ramachandron (%. residues)									
Most favored			97.4					98.4	
Additionally allowed			2.6					1.6	

[a] Only one crystal was used for each structure.
[b] Highest resolution shell is shown in parentheses.

NEMO helices, on both sides of this aperture. The IKK peptides are also mainly helical, except for an unwound region between 732 and 742, where the backbone is constrained by interactions between side chain tryptophans and main chain amides (Figures 4A and 4C). This highly constrained nonhelical region of the IKK peptide is unique and differentiates the NEMO/IKK association domain from other characterized 4-helix bundles such as the SNARE complexes (Fasshauer et al., 1998).

The IKK peptides themselves do not form a homodimer. Instead, each IKK peptide associates loosely with one of the

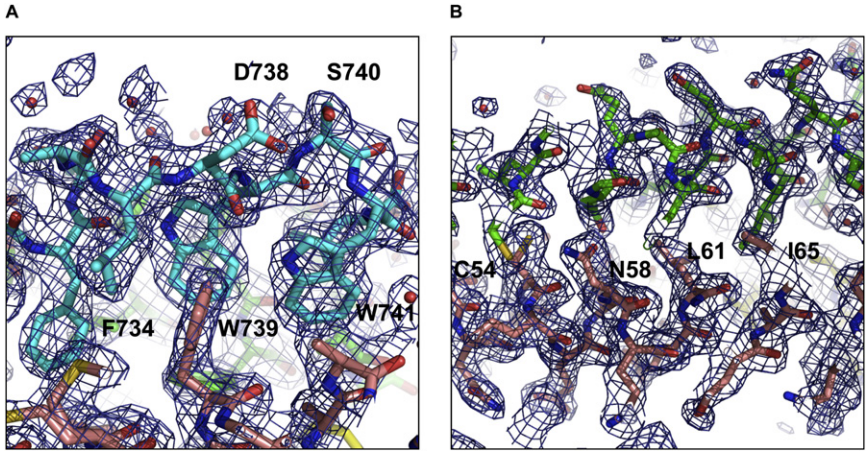

Figure 3. Final $2F_o - F_c$ Electron Density Map Contoured at 1.0 σ
(A) NBD region of IKKβ peptide.
(B) N-terminal NEMO dimerization region. Chains are color coded for NEMO (chain B, green; chain D, pink) and for IKKβ (chain A, blue; chain C, yellow).

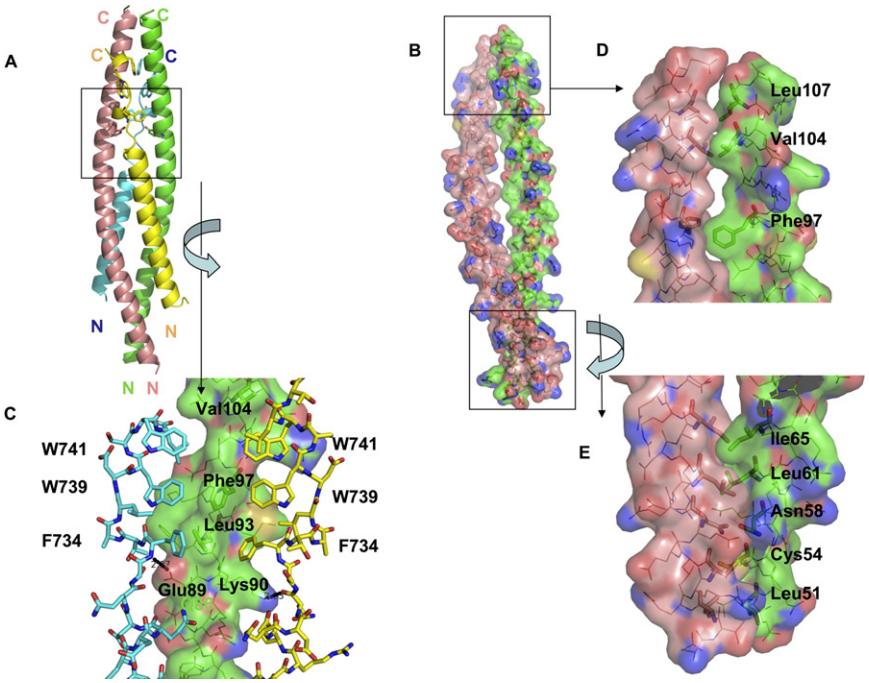

Figure 4. The NEMO/IKKβ Peptide Complex Is an Asymmetrical, Parallel Four-Helix Bundle

(A) Overall structure of the complex. NEMO chains (B and D; pink and green) form binding site for linker and NBD of IKK chains (A and C; blue and yellow). The box indicates the major site for IKK interaction.

(B) NEMO dimer showing the hole that results from stripping away IKK peptides.

(C) Close-up view of the IKK binding site with the three hydrophobic residues (734, 739, and 741) of IKK in sticks (blue and yellow) and NEMO residues that form the IKK-binding site (green surface).

(D) Close-up view of the NEMO dimerization patches at the C-terminal regions of the helix.

(E) Close-up view of the NEMO dimerization patches at the N-terminal regions of the helix.

NEMO molecules at the N terminus but is tightly wedged between the two molecules of the NEMO dimer at the C terminus. To best describe the interactions made by the IKK peptide we have assigned three regions within the peptide, designated as helical (705–731), linker (732–736), and the NBD (LDWSWL, 737–742) (Figure 6B). The flat slit of the dimeric NEMO forms two broad and extensive IKK-binding pockets, with approximate volume of 800 Å^3. These cavities are termed the specificity pockets and are lined by residues 85–101 of NEMO; each pocket is occupied by the IKK peptide linker and the NBD. In the text that follows, IKK residues are designated with a one-letter code, and NEMO residues are designated with a three-letter code.

The NEMO dimer is stabilized by hydrophobic interactions at the N and C termini (Figures 4B, 4D, and 4E). The N-terminal dimerization patch is more extensive with high degree of spatial and electrostatic complementarity (Figure 4E; Leu51:Leu51, Cys54:Cys54, Glu57:Arg62, Leu61:Leu61, and Ile65:Ile65). The Cβs of the Cys54 residues are separated by 4.35 Å, which is too long for a disulfide bond, because the ideal distance is 3.4–4.25A between Cβ positions (Hazes and Dijkstra, 1988). The C-terminal patch comprises only hydrophobic interfaces (Figure 4D; Leu103 and Val104: Leu103 and Val 104, Leu107:Leu107). Intriguingly, the NEMO dimer is not precisely symmetrical, because corresponding residues that form the C-terminal dimerization interface have different side chain rotamers. One Phe97 side chain forms the floor of the binding pocket for both peptides, and the other Phe97 forms the wall of the binding pocket for one of the peptides. The Arg101 side chain of chain C makes a salt bridge to the IKK peptide D738, but Arg101 of chain A does not make this interaction.

The NEMO specificity pocket forms few hydrogen-bond interactions with the IKK peptide but interacts mainly with hydrophobic side chains (F or M734, W739, and W741) (Figures 5A and 5B). The three hydrophobic side chains are oriented toward the specificity pocket and are organized by a unique IKK backbone conformation. The side chains of D738 and S740 in the NBD form a salt bridge that kinks the backbone. The side chains of the two tryptophans in the NBD sequence (W739 and W741) each form hydrogen bonds with backbone carbonyls in the IKK peptide (734 and 738, respectively). In an intermolecular interaction, the third hydrophobic residue, F734 or M734, is directed into the nonpolar pocket, and its backbone amide forms a hydrogen bond with Glu89 of NEMO (Figure 5C). These interactions result in the optimal placement of the three large IKK side chains inside the NEMO pocket, yielding a high-affinity complex. The intermolecular interactions between IKK and NEMO occur via hydrogen bonding (Ser85:Q730, Glu89:S733, and the F734 backbone amide, Arg101:D738) and hydrophobic interactions (Leu93:F734, Phe92:T735, Met94:F734, Phe97:W739, Ala100:W741, and Arg101:W741).

Conformational Similarity between the NEMO/IKKα/β Hybrid Peptide and NEMO/IKKβ Complexes

The two crystal structures described here contain selectivity regions consisting of the linker and NBD derived from either IKKα or IKKβ, but in both cases, the N-terminal helical region is derived from the IKKβ sequence (Figure 1B; Table 1). A superposition of the selectivity regions of these two structures indicates that the overall orientation of the four helices in the complex and the shapes of the NEMO cavities are essentially identical (Figure 5B). The overall RMSD of the Cαs of these two complexes is 1.13 Å for 203 α-carbons.

DISCUSSION

Organization and Implications for NEMO Regulation of IKK Activity

Although NEMO is a large scaffolding protein involved in a number of protein-protein interactions, we demonstrate here that a short stretch of residues in NEMO$_{44–111}$ is necessary and sufficient for IKK binding. The parallel arrangement of the helices observed in the minimal complex places conformational

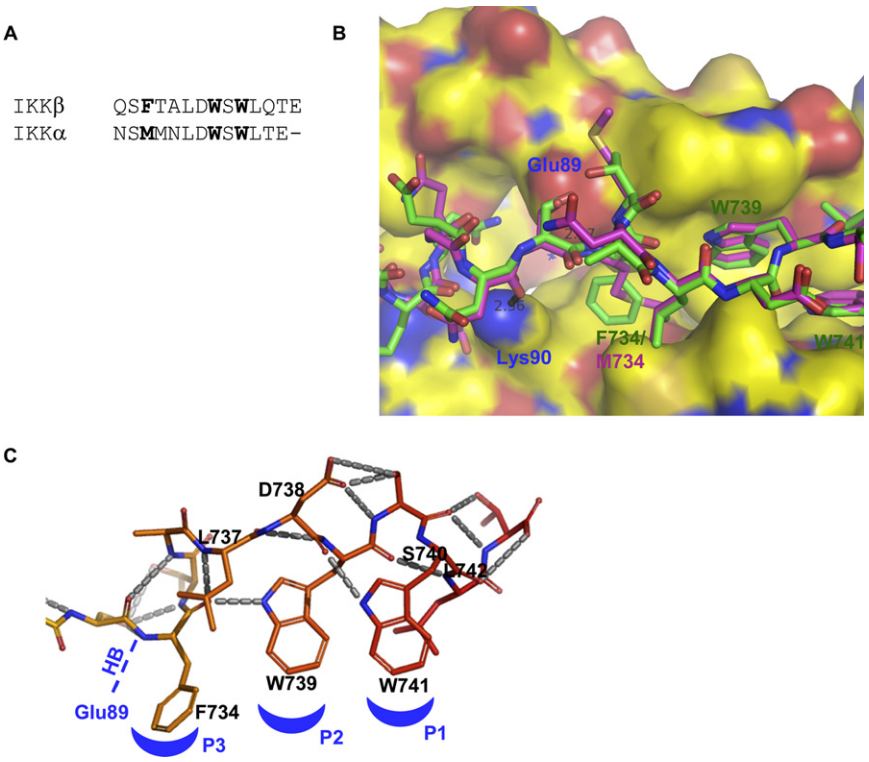

Figure 5. The Linker and NBD of IKKα and IKKβ Bind in a Hydrophobic Cleft

(A) Sequences of the linker and NBD for IKKα and IKKβ.

(B) Surface representation of NEMO with the superimposed NBD and linker segments of the IKKα/β hybrid peptide (magenta) and the IKKβ peptide (green). The surface is colored yellow for hydrophobic surfaces, red for negatively charged surfaces, and blue for positively charged surfaces. Note that three hydrophobic residues (734, 739, and 741) fit in the hydrophobic cleft. There is a similar hydrogen bond between E89 of NEMO and the 734 backbone amide of each IKK peptide.

(C) Intramolecular hydrogen bonding of the linker and NBD of the IKK peptide, which constrains the unique, unwound conformation. Included is a cartoon of the three hydrophobic pockets and the H-bond from Glu89 to the backbone of the IKK linker region, which defines the pharmacaphores of this binding site.

constraints on the full IKK complex. The regions involved in complex formation are at the N terminus of NEMO and the C terminus of the IKKα and IKKβ kinases. In addition, the kinases dimerize through leucine zipper motifs N-terminal to this region, and NEMO self-associates through leucine zipper motifs C-terminal to this region. Such a complex could be elongated and have a high apparent molecular weight by gel filtration, thus explaining the measurement of 700–900 kDa by others.

The minimal interaction region of NEMO forms a dimer and exhibits the same affinity for IKK peptides as does the larger $NEMO_{1–196}$ domain. Additionally, NEMO and IKK sequences are highly conserved across several mammalian species in both the NEMO dimerization regions and the IKK interaction regions, suggesting that that these regions indeed constitute the functional and structural core of the complex (Figure 6A). The NEMO hydrophobic residues in the specificity pocket would be exposed to water if one stripped the IKK peptides from the structure of the complex presented here, suggesting that the 44–111 region could be disordered, in a different conformation, or masked in the absence of IKK. Although we have no direct experimental evidence in support of any of these models, our NMR data on NEMO $_{44–111}$ do support the model that this region of NEMO becomes ordered in the presence of bound IKK peptide (Figure S2).

There are two intriguing features of the structure that may have implications for regulation of NEMO binding. First, in both the IKKα/β hybrid peptide and the IKKβ core complex structures, the two IKK peptides are not bound identically into the specificity pockets. The asymmetry is mainly due to a repositioning of NEMO side chain Phe97, which forms the floor of both specificity pockets. This suggests possible crosstalk between the two sites, on the basis of the orientation of the Phe97 side chain. Although the pockets are not structurally identical, they appear to bind two IKK peptides with similar affinity, because competition data can be adequately fit to a 1-site model (data not shown). Communication between binding sites within NEMO could possibly regulate their mutual IKK binding and/or release. Second, the structure shows that Ser68, whose mutation to the phosphoserine mimetic glutamate reduces dimerization and IKKβ binding (Palkowitsch et al., 2008), is buried in the hydrophobic core of the dimer. If this serine is phosphorylated as a result of NEMO regulation, it is unlikely to form a complex because of charge-charge repulsion.

NEMO has been shown to bind to IKKα, as well as IKKβ, although the interaction with IKKα has been reported to be weaker (May et al., 2002). Superimposing the structures of the NEMO/IKKα/β hybrid complex and the NEMO/IKKβ complex shows that the linker regions of IKKα and IKKβ are interchangeable (Figure 5B). The M734 and the F734 in the linker regions of IKKα and IKKβ, respectively, are equivalent in the manner in which they bind to the third hydrophobic site in the specificity pocket. This structural equivalence suggests that the difference in affinity between the IKKα and IKKβ kinases for NEMO could instead result from differences in the N-terminal helical region. We have shown that removing part or the entire helical region of the IKK peptides reduces their NEMO-binding affinity significantly. A noncanonical helix or a sequence with reduced helical propensity could also account for the reduced binding affinity of IKKα. The presence of helix-breakers G717 and G731 in IKKα may account for the reduced affinity of the IKKα kinase for NEMO (Figure 1B).

Importance of NBD Residues

The structure further provides an explanation for the effects of mutating the conserved NBD of IKK (LDWSWL) (May et al., 2002). Mutation of W to F at 739 or 741 can maintain the integrity of the structure and retain NEMO binding, but mutation of W to Y is tolerable only at position 739. In addition to forming specific

 ©2008 Elsevier Ltd All rights reserved

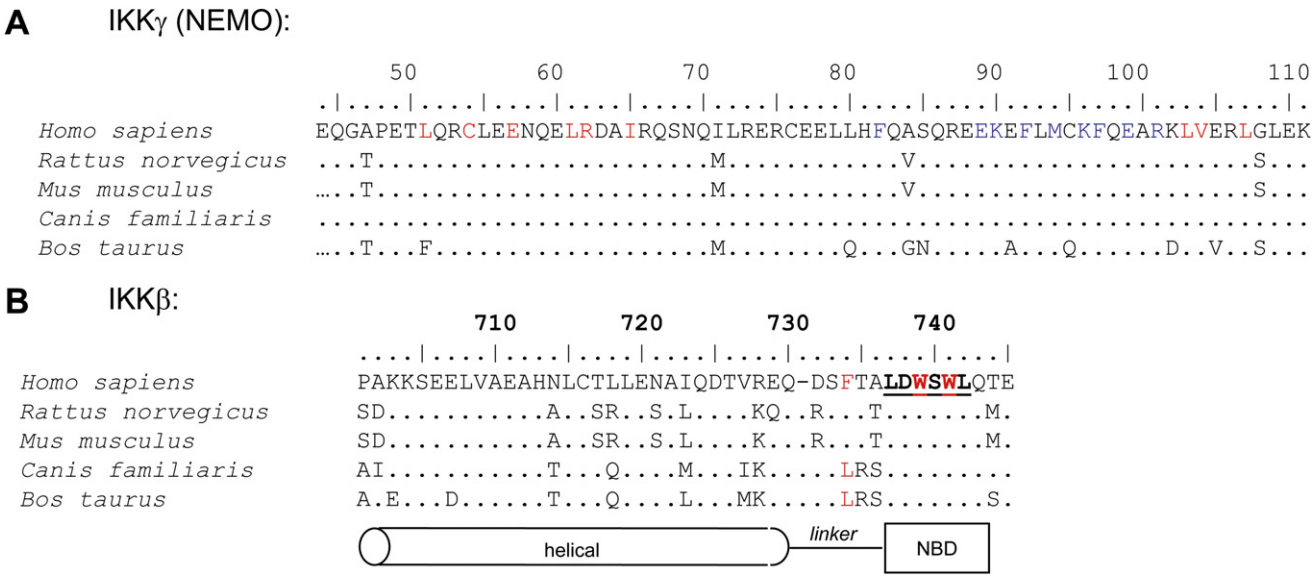

Figure 6. NEMO and IKK Sequence Alignments

(A) Sequence alignment of NEMO residues 44–111 from different mammalian species, highlighting deviations from the human sequence. The residues contributing to NEMO dimerization are in red, and residues involved in formation of the IKK specificity pocket are in blue.

(B) Sequence alignment of IKKβ residues 701–745 from different mammalian species denoting helical, linker, and NBD from the structure. The conserved hydrophobic residues that constitute a hot spot are shown in red.

hydrogen bonds to an IKK backbone, each tryptophan side chain of the NBD is buried in the nonpolar NEMO cavity forming aromatic interactions with Phe92 and Phe97. A mutation of W to F at 739 or 741 can maintain these interactions. However, Tyr will incur a desolvation penalty upon burial in this hydrophobic cavity and needs an appropriate hydrogen-bonding partner in the pocket. Our modeling studies show that the side chain hydroxyl of Y739 can form an additional intramolecular hydrogen bond with the backbone carbonyl of F734 and retain the native backbone IKK conformation. In contrast, Y741 does not have an appropriate hydrogen-bonding partner and will incur a desolvation penalty upon burial. Hence, the model predicts that introduction of a Y at 741 would destabilize the IKK conformation, leading to reduced NEMO binding.

The structure also explains why L737 or L742 is required in the NBD but mutation of both to alanine reduces binding. The structure suggests that both leucines form a seal around the trypophan side chains to reduce the access of waters, and they also help to wedge open the specificity pocket. It is possible that either leucine can perform these functions, but loss of both leucines is not tolerated.

Phosphorylation of the IKK C-terminal domain maintains IKK in a low, basal level of activity, possibly by reducing its interaction with NEMO (Karin and Delhase, 2000; Schomer-Miller et al., 2006). The structure explains this observation by identifying a critical S740 intermolecular interaction that can be affected by phosphorylation. On the basis of the structure, disruption of the IKK S740-D738 hydrogen bond by phosphorylation of S740 would alter the way the tryptophans could insert into the NEMO specificity pocket and thus reduce NEMO-binding affinity. Mutation of D738 to asparagine or glutamate, which can maintain this intramolecular interaction, retains NEMO binding, whereas its mutation to alanine, which cannot form this hydrogen bond, reduces NEMO-binding affinity (May et al., 2002).

Selectivity Pocket and Hot Spots

Three regions in the IKK peptide contribute to binding affinity for NEMO. However, the linker and NBD appear to form the more critical interactions: mutagenesis of two tryptophans in the conserved NBD causes a reduction in binding affinity of more than two orders of magnitude (May et al., 2002), and we found from the crystal structure that a hydrophobic residue from the linker region forms a third strong hydrophobic contact with NEMO. An alignment of the IKKβ sequences from many species shows that the hydrophobic residue at position 734 is conserved (Figure 6B). Furthermore, in the crystal structures, the M734 of the IKKα sequence occupies the same space as the F734 of IKKβ (Figure 5B). These observations lead us to propose a pharmacophore model consisting of three hydrophobic motifs derived from W741, W739, and M/F 734 side chains and a hydrogen bond donor mimicking the IKK 734 backbone amide, which interacts with Glu89, as a way of describing the important contacts needed in a small molecule or peptide-based inhibitor to recapitulate the properties of the bound IKK peptide (Figure 5C). Consequently, the critical interaction motif in IKK should be defined as being larger than the NBD (LDWSWL) motif previously cited (May et al., 2000).

The localization of key residues (M/F 734, W739, and W741) in a restricted area of the protein-protein interface and the effect of alanine substitutions on binding affinity (100-fold reduction in our assay for W739,741) define the region as a hot spot for the interaction (May et al., 2002). From a structural perspective, hot spots are near the geometric center of an interface and often contain the amino acids tryptophan, tyrosine, and arginine (Bogan and

Thorn, 1998). The NEMO/IKK interaction surface is quite extensive and removal of the IKK helix region provides a significant part of this binding energy (Figure 2C). However, disruption of these hot spot residues is sufficient to prevent the association (May et al., 2002). A second characteristic of a hot spot is the formation of a seal by residues surrounding the interface, which excludes water from the hydrophobic residues. In NEMO, this watertight seal is formed by side chains that interact with the exposed polar side chains of the peptide: Arg101 of NEMO with D738, Glu89 of NEMO with S733 and the 734 backbone amide, and Lys90 of NEMO with the 732 carbonyl. As a result, there are very few waters in the binding site as observed at 2.2 Å resolution. The sum of these characteristics of the binding interface suggests that the selectivity pocket, which binds the linker and NBD of IKK, could be the target of a small molecule therapeutic agent. Inhibition of IKK signaling by disruption of the NEMO/IKK interaction could be beneficial in a variety of autoimmune disorders and cancers; this work opens new avenues for the rational design and optimization of such molecules.

EXPERIMENTAL PROCEDURES

Protein Expression and Purification

DNA encoding the full-length $NEMO_{1–419}$ was obtained by PCR from the IMAGE clone 4651870. GST-NEMO expression vectors were generated by cloning NEMO-encoding fragments into pGEX-6p-1 (GE Healthcare). The proteins were produced in BL21(DE3) cells grown at 20°C and were induced with 1 mM isopropyl-β-D-thiogalactopyranoside (IPTG). Because of poor expression in the T7-based pGEX vector, GST-$NEMO_{1–419}$ and GST-$NEMO_{86–419}$ were subcloned into pBAD-HISA (Invitrogen) and were expressed in *E. coli* One Shot TOP 10 cells (Invitrogen) grown at 20°C and induced with 0.002% arabinose. Cells were lysed by French press, and clarified lysate was purified on Glutathione Sepharose 4 Fast Flow (GE Healthcare). GST-$NEMO_{1–196}$ was denatured with 10 M Guanidine-HCl, was refolded by dialysis into refolding buffer (10 mM TRIS [pH 8], 50 mM NaCl, 5 mM DTT, and 1 mM EDTA), and was purified by anion-exchange chromatography (Q Sepharose Fast Flow, GE Healthcare) followed by SEC (Superdex 200, GE Healthcare). GST-free $NEMO_{1–196}$ was made by cleaving the fusion protein with PreScission Protease enzyme (GE Healthcare) and removing GST and uncleaved GST-$NEMO_{1–196}$ with Glutathione Sepharose. Untagged $NEMO_{1–196}$ was denatured, refolded, and purified by anion-exchange and SEC, as described above for GST-$NEMO_{1–196}$.

Expression vectors for untagged NEMO proteins were generated by cloning NEMO encoding fragments into pET 11a, and for $NEMO_{44–111}$, a tryptophan was engineered at residue 45 for tracking the protein by UV absorbance. Protein was produced in BL21(DE3) cells grown at 37°C and induced with 1 mM IPTG. Selenomethionine-substituted $NEMO_{44–111}$ was produced B834 cells (methionine auxotroph, Novagen) using a standard procedure (Leahy et al., 1992) and was induced the same way. NEMO was isolated and solubilized from inclusion bodies (Supplemental Experimental Procedures) and was purified by reverse-phase chromatography on a Sep-Pak C8 column (Millipore).

Genes encoding IKKα/β hybrid and IKKβ (701–746) peptides were constructed by ligation of synthetic oligos, amplified, and cloned into pET32a (Novagen) for expression as His_6-thioredoxin fusion proteins containing an enterokinase cleavage site. The proteins were produced in BL21(DE3) cells as described above for $NEMO_{44–111}$ protein. Cells were lysed by stirring overnight in 8 M urea, 100 mM sodium phosphate, and 10 mM TRIS (pH 8.0) at 4°C. The fusion protein was purified from clarified lysate on Ni-NTA agarose (QIAGEN) in denaturing conditions; was refolded by dialysis against 50 mM TRIS (pH 8), 50 mM NaCl, and 5 mM 2-mercaptoethanol; and was cleaved with enterokinase (EMD Biosciences). The His-tagged thioredoxin portion was removed using Ni-NTA agarose, and the peptide was denatured with 8 M guanidinium hydrochloride and was further purified on a reverse-phase sep-pak C8 column.

IKK Synthetic Peptides

The IKK peptides were synthesized and purified at Mimotopes (sequences reported in Table 1). N-terminally biotinylated IKK α/β hybrid peptides 44-mer and 11-mer (Table 1) were synthesized by solid-phase synthesis using standard Fmoc/tBu protocol and were purified to greater than 95% homogeneity by RP-HPLC.

NEMO/Peptide Complex Preparation

For crystallization, $NEMO_{44–111}$ was denatured and refolded by dialysis as described for GST-$NEMO_{1–196}$. Sodium chloride (150 mM) and 1.1 molar excess lyophilized peptide were added to the protein, and the mixture was incubated at 37°C for 30 min and concentrated to 10 mg/ml. For NMR studies, NEMO/IKK peptide complexes were prepared by dissolving lyophilized $NEMO_{44–111}$ protein in an excess of IKK peptide dissolved in NMR buffer (50 mM phosphate buffer [pH 6.8], 95% H_2O and 5% D_2O, 50 mM NaCl, 0.02% NaN_3, and 5 mM DTT-D_{10}). The complex was then purified by size exclusion chromatography to ensure a 1:1 complex.

FRET Activity Assays

A FRET assay was used to detect NEMO peptide binding. In the direct binding format, 10 nM GST-NEMO was incubated with increasing amounts of biotinylated IKK peptide for 30 min at room temperature. The detection agent (50 nM streptavidin-conjugated APC and 10 nM LANCE™ Europium-W1024 labeled anti-GST, Perkin Elmer) was incubated for 30 min at room temperature, and the FRET signal was read on an LJL Analyst AD (Molecular Devices). In a competition format, 10 nM GST-$NEMO_{1–196}$ was bound to 200 nM biotinylated peptide in binding buffer.

Unlabeled peptides or untagged NEMO proteins were titrated into the mixture, incubated for 30 min at room temperature, and detected as described above.

Analytical Ultracentrifugation

Sedimentation equilibrium experiments were conducted at 20°C in a Beckman Optima XL-I ultracentrifuge (Beckman, Palo Alto, CA), using an An50 Ti 8-hole rotor and 12 mm six-channel charcoal-filled Epon centerpieces. Samples ranging in concentration from 0.05 to 0.7 mg/ml were centrifuged at 15,000, 22,000, and 30,000 rpm for $NEMO_{1–196}$, and 25,000 and 35,000 rpm for $NEMO_{44–111}$/IKKα/β hybrid complex. The sedimentation profiles were monitored at wavelengths of 228, 280, and 290 nm. Data were analyzed using the software NONLIN (Johnson et al., 1981), and molecular weights of the complexes were calculated using the program SEDNTERP (Laue et al., 1992).

SEC/Static Light-Scattering Analysis

SEC was performed using a 300 × 7.8 mm BioSep SEC 2000 column (Phenomenex) in 20 mM sodium phosphate (pH 7) and 150 mM NaCl (PBS) with a Waters Alliance HPLC instrument coupled to a refractive index detector (Waters, Milford, MA) and light-scattering detector (PD2000, Precison Detectors, Bellingham, MA). The weight average molar mass was determined using the Precision Detector Software. The system was calibrated using BSA assuming isotropic light scattering.

Nuclear Magnetic Resonance

The protein samples for NMR were uniformly labeled with ^{13}C, ^{2}H, or ^{15}N by growing cells in minimal salt media containing $^{13}C_6$-D-glucose and 99.9% D_2O and $^{15}NH_4Cl$ (Cambridge Isotope Laboratories, Spectra Stable Isotopes). NMR spectra were recorded on samples of concentration varying between 0.1 and 0.6 mM, at 35°C. All data were acquired on a Bruker Avance600 spectrometer equipped with a cryogenic probe. Construct screening utilized ^{15}N-labeled protein and ^{1}H,^{15}N-HSQC (Bax et al., 1983) or ^{1}H-^{15}N-TROSY (Pervushin et al., 1997) experiments.

Crystallization and Structure Solution

Crystals of NEMO/IKK α/β hybrid peptide complex were formed under silicon oil using 1:1 volume ratio of 10 mg/ml protein solution to crystallization solution of 35% Peg 8K, 0.1 M Tris (pH 8), 0.2 M ammonium chloride, and 10 mM dithiothreitol (DTT). The crystals were cryoprotected in 35% Peg4K, 10% ethylene glycol, 0.1 M Tris (pH 8), 0.1 M ammonium chloride, and 10 mM DTT

 ©2008 Elsevier Ltd All rights reserved

transferred into liquid nitrogen. Crystals of the NEMO/IKKβ peptide complex were grown in vapor-diffusion hanging-drop set-up at 20°C using 1:1 volume ratio of 10 mg/ml complex with a well solution of 30% Peg 4K, 0.1 M Tris (pH 8.5), 0.2 M $MgCl_2$, 10 mM DTT, and 1.4 mM deoxybigchap. The crystals were cryoprotected in 30% Peg4K, 0.1 M Tris (pH 8.5), 0.2 M $MgCl_2$, 10 mM DTT, and 10% glycerol and were transferred into liquid nitrogen.

The crystals belong to space group $P2_12_12_1$ with unit cell dimensions as follows: a = 42.1Å, b = 105.6 Å, c = 56.8 Å, and $\alpha = \beta = \gamma = 90°$, which are consistent with a 2:2 ratio of NEMO and IKK peptide molecules per asymmetric unit (Table 2). Native data were collected at beamline X8C at the National Synchrotron Light Source (Upton, NY) at wavelength 1.1 Å. Two MAD experiments were conducted on selenomethionine-NEMO/unlabeled IKK α/β hybrid peptide complex crystals using three or four wavelengths near the selenium K edge (Table 2). Data processing to 2.5 Å was performed with the HKL2000 (Otwinowski and Minor, 1997) program package. The structure of the NEMO/IKK α/β hybrid complex was solved by multiple anomalous dispersion phasing using SOLVE (Terwilliger and Berendzen, 1999), which identified two selenium sites per asymmetric unit and produced phases with a figure of merit of 0.70 to 3.2Å. Solvent flattening with RESOLVE (Terwilliger and Berendzen, 1999) using a solvent content of 60% resulted in an improvement in phasing with an overall figure of merit of 0.79 to 3.2 Å. The initial model was traced by hand, using O software (version 8) (Jones et al., 1991), and was subjected to rounds of refinement using an MLHL target and reserving 5% of the reflections for the test set. The availability of native data to 2.25 Å resolution allowed re-refinement against an MLF target and refinement proceeded to convergence. The structure was then refined with REFMAC5 (Murshudov et al., 1997) and by removing side chains with low occupancy. The last cycles of refinement were performed with TLS restraints as implemented in REFMAC5 in which the optimal number of groups was defined according to TLS Motion Determination (version 0.8.1) (Painter and Merritt, 2006a, 2006b). The final model of the NEMO/IKK α/β hybrid complex has an R factor of 23.7% and an R_{free} of 28.1% and consists of residues B49–B109 and D49–D110 of NEMO (chains B and D), residues A705–A743 and N-terminal Met-Ala-C701–C743 of the IKK peptide (chains A and C), and 62 waters. The Wilson plot overall B for this complex is 70.6 $Å^2$.

The NEMO/IKKβ peptide complex structure was solved by molecular replacement using the NEMO/ IKK α/β hybrid complex structure as a search model in MOLREP (Vagin and Teplyakov, 1997) and was refined as described above for the hybrid complex. The final model of the NEMO/IKKβ complex has an R factor of 20.8% and an R_{free} of 29.4% and consists of residues B49–B109 and D49–D110 of NEMO (chains B and D), residues A705–A743 and C702–C743 of the IKKβ peptide (chains A and C), and 103 waters. The Wilson plot overall B for this complex is 43.9 $Å^2$. The quality of the two models was analyzed by PROCHECK (Laskowski et al., 1993) (Table 2).

ACCESSION NUMBERS

The coordinates for the NEMO/IKKβ and NEMO/IKKα/β hybrid complexes have been deposited into the Protein Data Bank with the codes 3BRV and 3BRT, respectively.

SUPPLEMENTAL DATA

Supplemental Data include two figures and Supplemental Experimental Procedures, and can be found with this article online at http://www.structure.org/cgi/content/full/16/5/798/DC1/.

ACKNOWLEDGMENTS

We gratefully acknowledge Milka Yanchikova and Stephano Liparoto, for experimental assistance, and Chris Fitch and Ami Horne, for optimizing crystals. We are indebted to Ann Boriack-Sjodin for MAD data collection of the $NEMO_{44–111}$/IKKα/b hybrid complex. Data collection of both complexes occurred at the X25 and X8C beamlines at Brookhaven National Laboratories. We are indebted to Alan Corin, Jessica Friedman, Serene Josiah, Herman Van Vlijmen, Adrian Whitty, Véronique Bailly, Mitch Reff, and Blake Pepinsky for guidance and support.

Received: October 24, 2007
Revised: January 22, 2008
Accepted: February 2, 2008
Published: May 6, 2008

REFERENCES

Agou, F., Ye, F., Goffinont, S., Courtois, G., Yamaoka, S., Israel, A., and Veron, M. (2002). NEMO trimerizes through its coiled-coil C-terminal domain. J. Biol. Chem. *277*, 17464–17475.

Bax, A., Griffey, R.H., and Hawkins, B.L. (1983). Correlation of proton and nitrogen-15 chemical shifts by multiple quantum NMR. J. Magn. Reson. *55*, 301–315.

Biswas, D.K., Shi, Q., Baily, S., Strickland, I., Ghosh, S., Pardee, A.B., and Iglehart, J.D. (2004). NF-κB activation in human breast cancer specimens and its role in cell proliferation and apoptosis. Proc. Natl. Acad. Sci. USA *101*, 10137–10142.

Bogan, A.A., and Thorn, K.S. (1998). Anatomy of hot spots in protein interfaces. J. Mol. Biol. *280*, 1–9.

Bonizzi, G., and Karin, M. (2004). The two NF-κB activation pathways and their role in innate and adaptive immunity. Trends Immunol. *25*, 280–288.

Combet, C., Blanchet, C., Geourjon, C., and Deleage, G. (2000). NPS@: network protein sequence analysis. Trends Biochem. Sci. *25*, 147–150.

DiDonato, J.A., Hayakawa, M., Rothwarf, D.M., Zandi, E., and Karin, M. (1997). A cytokine-responsive IκB kinase that activates the transcription factor NF-κB. Nature *388*, 548–554.

Fasshauer, D., Sutton, R.B., Brunger, A.T., and Jahn, R. (1998). Conserved structural features of the synaptic fusion complex: SNARE proteins reclassified as Q- and R-SNAREs. Proc. Natl. Acad. Sci. USA *95*, 15781–15786.

Fontan, E., Traincard, F., Levy, S.G., Yamaoka, S., Veron, M., and Agou, F. (2007). NEMO oligomerization in the dynamic assembly of the IκB kinase core complex. FEBS J. *274*, 2540–2551.

Ghosh, S., and Karin, M. (2002). Missing pieces in the NF-κB puzzle. Cell Suppl. *109*, S81–S96.

Hazes, B., and Dijkstra, B.W. (1988). Model building of disulfide bonds in proteins with known three-dimensional structure. Protein Eng. *2*, 119–125.

Johnson, M.L., Correia, J.J., Yphantis, D.A., and Halvorson, H.R. (1981). Analysis of data from the analytical ultracentrifuge by nonlinear least-squares techniques. Biophys. J. *36*, 575–588.

Jones, T.A., Zou, J.Y., Cowan, S.W., and Kjeldgaard, M. (1991). Improved methods for building protein models in electron density maps and the location of errors in these models. Acta Crystallogr. A *47*, 110–119.

Karin, M. (1999). How NF-κB is activated: the role of the IκB kinase (IKK) complex. Oncogene *18*, 6867–6874.

Karin, M., and Delhase, M. (2000). The IκB kinase (IKK) and NF-κB: key elements of proinflammatory signalling. Semin. Immunol. *12*, 85–98.

Laskowski, R.A., MacArthur, M.W., Moss, D.S., and Thornton, J.M. (1993). PROCHECK: a program to check the stereochemical quality of protein structures. J. Appl. Cryst. *26*, 283–291.

Laue, T.M., Shah, B.D., Ridgeway, T.M., and Pelletier, S.L. (1992). Computer-aided interpretation of sedimentation data for proteins. In Analytical Ultracentrifugation in Biochemistry and Polymer Science, S.A. Harding, A.J. Rowe, and J.C. Horton, eds. (Cambridge: Royal Society of Chemistry), pp. 63–89.

Leahy, D.J., Hendrickson, W.A., Aukhil, I., and Erickson, H.P. (1992). Structure of a fibronectin type III domain from tenascin phased by MAD analysis of the selenomethionyl protein. Science *258*, 987–991.

Leonardi, A., Chariot, A., Claudio, E., Cunningham, K., and Siebenlist, U. (2000). CIKS, a connection to IκB kinase and stress-activated protein kinase. Proc. Natl. Acad. Sci. USA *97*, 10494–10499.

Makris, C., Godfrey, V.L., Krahn-Senftleben, G., Takahashi, T., Roberts, J.L., Schwarz, T., Feng, L., Johnson, R.S., and Karin, M. (2000). Female mice heterozygous for IKK gamma/NEMO deficiencies develop a dermatopathy similar to the human X-linked disorder incontinentia pigmenti. Mol. Cell *5*, 969–979.

 ©2008 Elsevier Ltd All rights reserved

Marienfeld, R.B., Palkowitsch, L., and Ghosh, S. (2006). Dimerization of the IκB kinase-binding domain of NEMO is required for tumor necrosis factor α-induced NF-κB activity. Mol. Cell. Biol. *26*, 9209–9219.

May, M.J., D'Acquisto, F., Madge, L.A., Glockner, J., Pober, J.S., and Ghosh, S. (2000). Selective inhibition of NF-κB activation by a peptide that blocks the interaction of NEMO with the IκB kinase complex. Science *289*, 1550–1554.

May, M.J., Marienfeld, R.B., and Ghosh, S. (2002). Characterization of the IκB-kinase NEMO binding domain. J. Biol. Chem. *277*, 45992–46000.

Mercurio, F., Zhu, H., Murray, B.W., Shevchenko, A., Bennett, B.L., Li, J., Young, D.B., Barbosa, M., Mann, M., Manning, A., et al. (1997). IKK-1 and IKK-2: cytokine-activated IκB kinases essential for NF-κB activation. Science *278*, 860–866.

Murshudov, G.N., Vagin, A.A., and Dodson, E.J. (1997). Refinement of macromolecular structures by the maximum-likelihood method. Acta Crystallogr. D Biol. Crystallogr. *53*, 240–255.

Otwinowski, Z., and Minor, W. (1997). Processing of X-ray diffraction data collected in oscillation mode. In Methods in Enzymology, Macromolecular Crystallography Part A, C.W. Carter and R.M. Sweet, eds. (New York: Academic Press), pp. 307–326.

Page, R., Peti, W., Wilson, I.A., Stevens, R.C., and Wuthrich, K. (2005). NMR screening and crystal quality of bacterially expressed prokaryotic and eukaryotic proteins in a structural genomics pipeline. Proc. Natl. Acad. Sci. USA *102*, 1901–1905.

Painter, J., and Merritt, E.A. (2006a). Optimal description of a protein structure in terms of multiple groups undergoing TLS motion. Acta Crystallogr. D Biol. Crystallogr. *62*, 439–450.

Painter, J., and Merritt, E.A. (2006b). TLSMB web server for the generation of multi-group TLS models. J. Appl. Cryst. *39*, 109–111.

Palkowitsch, L., Leidner, J., Ghosh, S., and Marienfeld, R.B. (2008). Phosphorylation of serine 68 in the IκB kinase (IKK)-binding domain of NEMO interferes with the structure of the IKK complex and tumor-necrosis-factor-α-induced NF-κB activity. J. Biol. Chem. *283*, 76–86.

Pervushin, K., Riek, R., Wider, G., and Wuthrich, K. (1997). Attenuated T2 relaxation by mutual cancellation of dipole-dipole coupling and chemical shift anisotropy indicates an avenue to NMR structures of very large biological macromolecules in solution. Proc. Natl. Acad. Sci. USA *94*, 12366–12371.

Rudolph, D., Yeh, W.C., Wakeham, A., Rudolph, B., Nallainathan, D., Potter, J., Elia, A.J., and Mak, T.W. (2000). Severe liver degeneration and lack of NF-κB activation in NEMO/IKKγ-deficient mice. Genes Dev. *14*, 854–862.

Schmidt-Supprian, M., Bloch, W., Courtois, G., Addicks, K., Israel, A., Rajewsky, K., and Pasparakis, M. (2000). NEMO/IKK γ-deficient mice model incontinentia pigmenti. Mol. Cell *5*, 981–992.

Schomer-Miller, B., Higashimoto, T., Lee, Y.K., and Zandi, E. (2006). Regulation of IκB kinase (IKK) complex by IKKγ-dependent phosphorylation of the T-loop and C terminus of IKKβ. J. Biol. Chem. *281*, 15268–15276.

Solt, L.A., Madge, L.A., Orange, J.S., and May, M.J. (2007). Interleukin-1-induced NF-κB activation is NEMO-dependent but does not require IKKβ. J. Biol. Chem. *282*, 8724–8733.

Tas, S.W., Vervoordeldonk, M.J., Hajji, N., May, M.J., Ghosh, S., and Tak, P.P. (2006). Local treatment with the selective IκB kinase β inhibitor NEMO-binding domain peptide ameliorates synovial inflammation. Arthritis Res. Ther. *8*, R86.

Tegethoff, S., Behlke, J., and Scheidereit, C. (2003). Tetrameric oligomerization of IκB kinase γ (IKKγ) is obligatory for IKK complex activity and NF-κB activation. Mol. Cell. Biol. *23*, 2029–2041.

Terwilliger, T.C., and Berendzen, J. (1999). Automated MAD and MIR structure solution. Acta Crystallogr. D Biol. Crystallogr. *55*, 849–861.

Thomas, R.P., Farrow, B.J., Kim, S., May, M.J., Hellmich, M.R., and Evers, B.M. (2002). Selective targeting of the nuclear factor-κB pathway enhances tumor necrosis factor-related apoptosis-inducing ligand-mediated pancreatic cancer cell death. Surgery *132*, 127–134.

Vagin, A., and Teplyakov, A. (1997). MOLREP: an automated program for molecular replacement. J. Appl. Cryst. *30*, 1022–1025.

Wolf, E., Kim, P.S., and Berger, B. (1997). MultiCoil: a program for predicting two- and three-stranded coiled coils. Protein Sci. *6*, 1179–1189.

Woronicz, J.D., Gao, X., Cao, Z., Rothe, M., and Goeddel, D.V. (1997). IκB kinase-β: NF-κB activation and complex formation with IκB kinase-α and NIK. Science *278*, 866–869.

Yamaoka, S., Courtois, G., Bessia, C., Whiteside, S.T., Weil, R., Agou, F., Kirk, H.E., Kay, R.J., and Israel, A. (1998). Complementation cloning of NEMO, a component of the IκB kinase complex essential for NF-κB activation. Cell *93*, 1231–1240.

Zandi, E., Rothwarf, D.M., Delhase, M., Hayakawa, M., and Karin, M. (1997). The IκB kinase complex (IKK) contains two kinase subunits, IKKα and IKKβ, necessary for IκB phosphorylation and NF-κB activation. Cell *91*, 243–252.

Zandi, E., Chen, Y., and Karin, M. (1998). Direct phosphorylation of IκB by IKKα and IKKβ: discrimination between free and NF-κB-bound substrate. Science *281*, 1360–1363.

 ©2008 Elsevier Ltd All rights reserved